PARAMETRIC ANALYSIS OF SURFACES OF ACOUSTO-ELECTRONIC RESONATORS USING NI LABVIEW AND SCANNING PROBE MICROSCOPY

Ph.D. V.V. Spiridonov

Baltic State Technical University «VOENMEH» named after D.F. Ustinov, Saint Petersburg, Russia

E-mail: spiridonov-vlad@yandex.ru

Abstract: *The article describes the results of analysis of the two acoustic electronic resonators performed using the scanning probe microscope and the software developed in the graphical integrated development environment LabVIEW with the machine vision module NI LabVIEW Vision. The most important surface parameters were measured and analyzed, and the corresponding conclusions were made regarding possible defects and compliance with the reference performance indicators of the two resonators.*

Keywords: QUALITY, RESONATORS, MACHINE VISION, HISTOGRAM EQUALIZATION, LABVIEW

1. Introduction

Today, acousto-electronic devices are widely used in radio-electronic devices, including mobile communication devices, radar systems, and radio navigation equipment. Among huge variety of acousto-electronic devices, one of the most promising are SAW resonators which operate on the basis of Surface Acoustic Waves. These resonators are highly sensitive, and can efficiently detect and handle complex signals in real-time or near real-time [1]. However, accuracy and sensitivity of SAW resonators strongly depend on the quality and geometry of their surfaces.

In this paper, surfaces of the two acousto-electronic SAW resonators were analyzed using a scanning probe microscope, NI LabVIEW Vision library, and the special LabVIEW-based software developed at BSTU VOENMEH.

2. Analysis workflow

To acquire images of the resonator surfaces, the special test equipment based on Nanoeducator, a popular scanning probe microscope (SPM), is used. The information acquired from the Nanoeducator is saved as an SPM frame, which is a two-dimensional array (matrix) of integers *Z [i, j]*. Each pair of indices *<i, j>* corresponds to a certain point of the surface within the scanned area. Coordinates of the surface points are calculated by multiplying the corresponding index by the distance between the points at which the data was acquired. SPM-frames are visualized by as two-dimensional (2D) and three-dimensional (3D) brightness-based images, which are convenient for edge detection. For 2D visualization, each point *Z = f (x, y)* of the surface is mapped with a hue of a certain color depending on the height of the surface item at that point. For 3D visualization, the whole image of the surface is generated in the axonometric perspective using pixels or lines. To ensure efficient coloring of 3D images and highlight even the smallest items on the surfaces, a point light source located above the surface was used.

To facilitate and speed up the image processing, as well as to filter out unwanted ("noisy") particles on the background and along the image border, it is necessary to binarize the image using local thresholds and/or apply corresponding particle filters. Image binarization in LabVIEW can be performed with the **IMAQ Threshold** component from NI Vision library [2]. The simplified program code of the algorithm is shown in Fig. 1.

Before the analysis, the image should be equalized using histogram alignment and the transformation function, which can be derived from a histogram of the original image. Assume that a given image with the first histogram is equalized using the following equation:

$$s = T(r) = \int_0^r p_r(w)dw, \quad (1)$$

where $p_r(r)$ and $p_z(r)$ are the original and target probability-density functions of brightness respectively, and w is the brightness.

If we assume that the target image is available, then its brightness levels could also be aligned using the conversion function:

$$v = G(z) = \int_0^z p_z(w)dw, \quad (2)$$

where $p_r(r)$ and $p_z(r)$ are the original and target probability-density functions of brightness respectively, and w is the brightness.

Therefore, the inverse transformation $z = G^{-1}(v)$ would restore the original levels, with $p_s(s)$ and $p_v(v)$ being identical uniform densities, since the equations (1) and (2) mutually ensure uniform density regardless of the nature of the probability-density function under the integral sign. Thus, if we replace v in the inverse transformation with the inverse levels s obtained from the original image, the resulting levels $z = G^{-1}(s)$ will have the desired probability-density function $p_z(z)$. If we assume that $G^{-1}(s)$ is a single-value function, the high-level algorithm can be described as follows [3]:

1. Align the brightness levels of the original image using equation (1).
2. Determine the desired brightness probability-density function and obtain the transformation function $G(z)$ using equation (2).
3. Perform the inverse transformation $z = G^{-1}(s)$ of the image to the brightness levels of the image with the histogram aligned in Step 1.

The proposed algorithm is implemented in the LabVIEW environment using NI Vision library (Fig. 2).

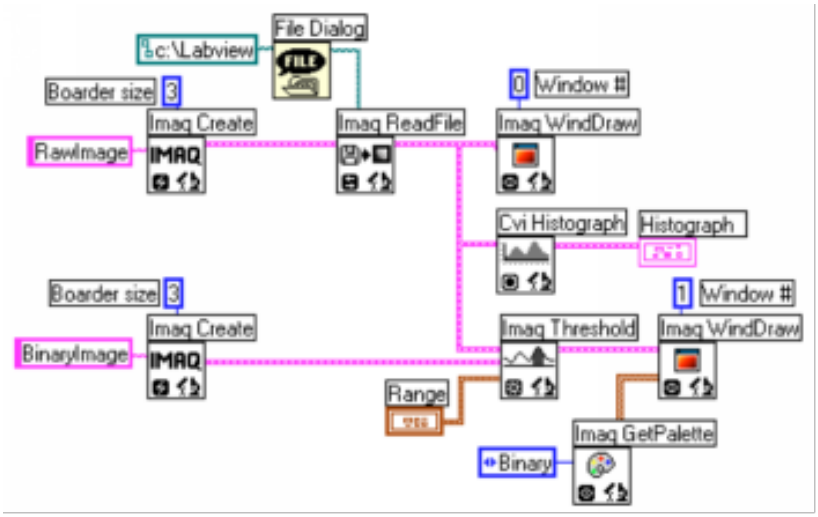

***Fig. 1**. Simplified program code of the image binarization algorithm*

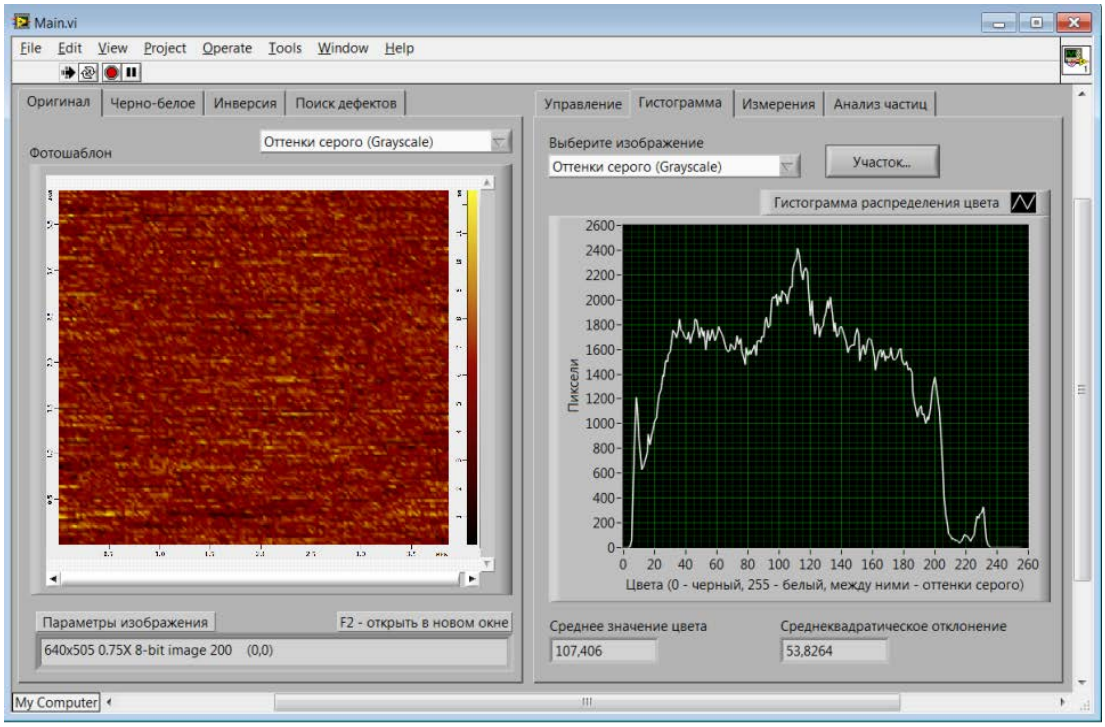

***Fig. 2**. Screenshot of the developed LabVIEW-based software*

3. Toolkit used for analysis

To analyze the images acquired from the scanning probe microscope, a software tool developed in the LabVIEW environment using the NI LabVIEW Vision library was used.

The software itself is a virtual instrument (VI) consisting of the two parts - the Front Panel and the Block Diagram. The Front Panel implements the graphical user interface, while the Block Diagram implements the internal logic of the software (its source code) [4, 5].

The software provides the following key features:

1. Operations with images in four main formats (BMP, JPEG, PNG, TIFF)
2. Image transformation: negative image, decomposition into color channels (Red, Green, Blue), grayscale image, binary image, inverted binary image
3. Measurement of distances between the two user-defined points, as well as any rectangular and annular areas in the image
4. Image calibration (setting up of a reference distance for scaling)
5. Calculation of the basic statistical parameters of a surface
6. Histograms of brightness, both for the whole image and for any user-defined area, as well as the calculation of the average brightness and standard deviation
7. Particle ("blob") analysis of the image and calculation of numerous particle parameters (length, height, area, center of gravity, etc.).

4. Results of the analysis

The following resonators were analyzed (Fig. 3 and Fig. 4):

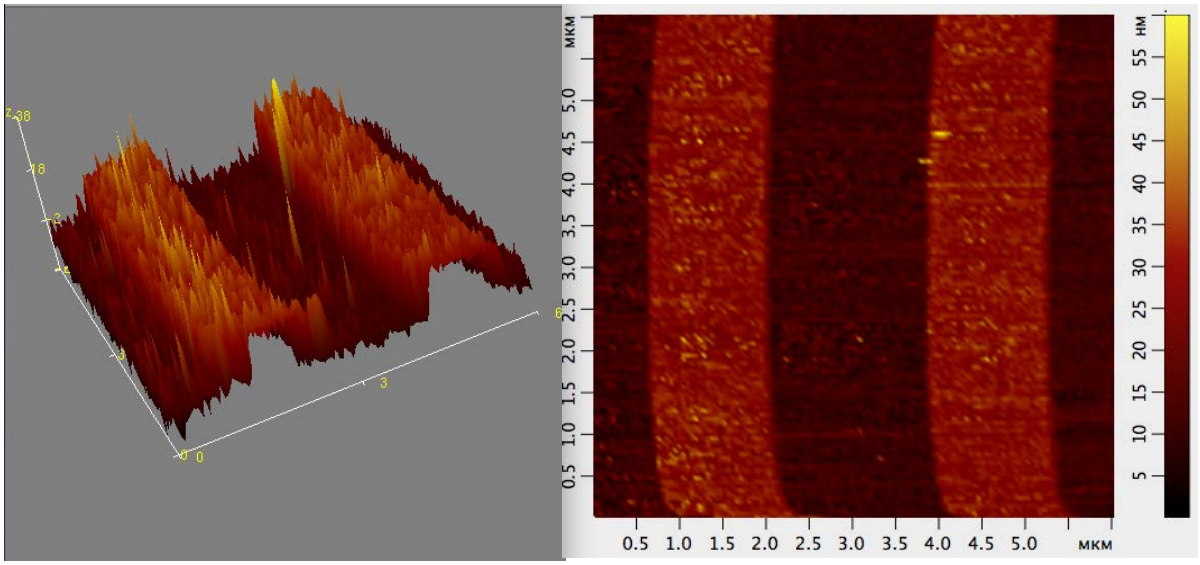

Fig. 3. *Resonator #1 (3D and 2D views)*

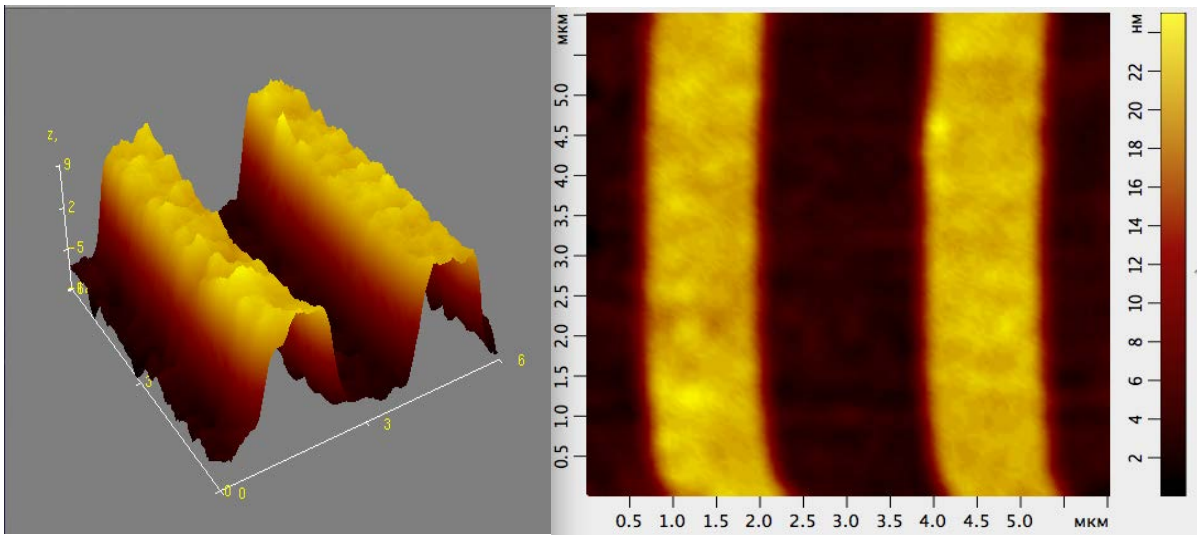

Fig. 4. *Resonator #2 (3D and 2D views)*

These resonators normally should have the reference characteristics listed in Table 1.

Table 1: Reference parameters of the two acousto-electronic resonators

Parameter name and its measurement unit	Short designation	Reference value for Resonator #1	Reference value for Resonator #2
Transformation range, g	D_g	± 25	± 50
Sensitivity threshold, g	E_g	0.3	0.6
Min. non-linearity of transfer characteristics, %	E	5	5
Conversion frequency range, Hz	F	50	75
Supply voltage, V	U_{in}	5	5
Max. amplitude of the output signal, V	U_{out}	1	1

The actual statistical values obtained during the analysis are summarized in Table 2.

Table 2: Statistical values of surfaces of the two acousto-electronic resonators

Parameter	Resonator #1	Resonator #2
Average unevenness	481.13 nm	513.40 nm
Minimum unevenness	19.61 nm	0.00 nm
Maximum unevenness	1000.00 nm	1000.00 nm
Median unevenness	498.04 nm	498.04 nm
Asymmetry	-0.576	0.349
Excess	6.03	1.84
Surface area	$10.18 * 10^{-9}$ m^2	$8.63 * 10^{-9}$ m^2
Projection area	$9.88 * 10^{-9}$ m^2	$8.40 * 10^{-9}$ m^2
Slope θ	0.24 degrees	0.38 degrees
Slope φ	-142.83 degrees	-140.07 degrees

5. Conclusions

Based on the obtained results, the following conclusions can be made:

1. Despite that Resonator #1 is characterized by a smaller absolute height difference than Resonator #2, the standard deviation of the unevenness heights of Resonator #1 is much larger than that of the Resonator #2, which indicates an uneven distribution of these heights on the surface of Resonator #1. Thus, the surface of Resonator #2 demonstrates higher irregularities, but at the same time it is much smoother and does not have any sharp peaks.
2. The values of asymmetry of surfaces of the both resonators are very different. This indicates that Resonator #1 demonstrates deeper cavities (negative asymmetry), i.e. its surface is rather "porous", while Resonator #2 shows sharp peaks without numerous cavities.
3. The values of the excess of surfaces of the both resonators are also different. This means that the surface profile of Resonator #1 features *elongated and narrow* peaks ("barbs") and cavities (Excess > 3), while Resonator #2 has *wider and low-sloped* peaks and cavities (Excess < 3).
4. Based on the above three conclusions, the quality of the surface of Resonator #2 is significantly higher than that of Resonator #1, and can be characterized as symmetric and smooth thanks to the absence of sharp peaks ("barbs") and sharp cavities ("pores"). The observed deviations may lead to deviations in the operating frequency of Resonator #1 compared to the reference values.

References

[1] Acousto-electronic devices. Terms and definitions / Acoustic wave devices. Terms and definitions [Text]: *International Standard GOST 28170-89 - 1989. - Introduction. 1991-01-01. Moscow: Publishing house of standards*, 2007.

[2] Y.V. Wisilter. Processing and analysis of digital images with examples on LabVIEW and IMAQ Vision [Text]: *Moscow: DMK Press, 2007* - 464 p.

[3] V.V. Spiridonov. Analysis and implementation of the micro-level defects detection method [Text]: *Materials of the 67th Scientific and Practical Conference SPBGETU LETI - SPBGETU LETI*, 2012 - 189 p.

[4] System for automated visual inspection for the engineering instrumentation industry [Text]: *Certificate of state registration of the computer program No.2014610514* / V. V. Spiridonov.

[5] V.V. Spiridonov. Key segmentation methods of grayscale images in modern machine vision systems [Text]: *Materials of the III All-Russian Scientific and Technological Conference "Basic Principles of Ballistic Design"* – Publishing house of BSTU "VOENMEH", 2012, Vol.2 - 428 p.